

Supersolid phase in a $U(2)$ symmetric $S = 1$ magnet on the triangular lattice

Si-Cheng Wang(王思成) and Zheng-Xin Liu(刘正鑫)

Citation: Chin. Phys. B, 2026, 35 (**4**): 047506. DOI: 10.1088/1674-1056/ae3604
http://cpb.iphy.ac.cn; http://iopscience.iop.org/cpb

What follows is a list of articles you may be interested in

Hall anomalies in the centrosymmetric triangular-lattice antiferromagnet $GdGa_2$

Sidi Wang(王思迪), Jiyuan Li(李纪源), Yuhao Wang(王宇豪), Keqi Xia(夏克奇), Jing Meng(孟婧), Bocheng Yu(余博丞), Yiqian Hu(胡艺骞), Zheng Li(李峥), Hui Zhang(张慧), Jingzhong Luo(罗晶中), Dongmei Jiang(蒋冬梅), Qingfeng Zhan(詹清峰), Tian Shang(商恬), and Yang Xu(徐杨)
Chin. Phys. B, 2026, 35 (**2**): 027502. DOI: 10.1088/1674-1056/ae2672

Orbital magnetic field effect on spin waves in a triangular lattice tetrahedral antiferromagnetic insulator

Pi-Ye Zhou(周丕烨), Xiao-Hui Li(李晓慧), and Yuan Wan(万源)
Chin. Phys. B, 2025, 34 (**6**): 067501. DOI: 10.1088/1674-1056/adca1f

Auxiliary-field Monte Carlo method for frustrated spin systems

Ning Cai(蔡凝), Yuan Gao(高源), Wei Li(李伟), and Yang Qi(戚扬)
Chin. Phys. B, 2025, 34 (**2**): 027504. DOI: 10.1088/1674-1056/ada758

Structure and frustrated magnetism of the two-dimensional triangular lattice antiferromagnet $Na_2BaNi(PO_4)_2$

Fei Ding(丁飞), Yongxiang Ma(马雍翔), Xiangnan Gong(公祥南), Die Hu(胡蝶), Jun Zhao(赵俊), Lingli Li(李玲丽), Hui Zheng(郑慧), Yao Zhang(张耀), Yongjiang Yu(于永江), Lichun Zhang(张立春), Fengzhou Zhao(赵风周), and Bingying Pan(泮丙营)
Chin. Phys. B, 2021, 30 (**11**): 117505. DOI: 10.1088/1674-1056/abff1d

Crystal growth and magnetic properties of quantum spin liquid candidate $KErTe_2$

Weiwei Liu(刘维维), Dayu Yan(闫大禹), Zheng Zhang(张政), Jianting Ji(籍建葶), Youguo Shi(石友国), Feng Jin(金峰), and Qingming Zhang(张清明)
Chin. Phys. B, 2021, 30 (**10**): 107504. DOI: 10.1088/1674-1056/ac1574

RAPID COMMUNICATION

Supersolid phase in a $U(2)$ symmetric $S = 1$ magnet on the triangular lattice

Si-Cheng Wang(王思成)[1,2,3] and Zheng-Xin Liu(刘正鑫)[1,4,†]

[1] *Department of Physics and Beijing Key Laboratory of Opto-electronic Functional Materials and Micro-nano Devices, Renmin University of China, Beijing* 100872, *China*

[2] *Beijing National Laboratory for Condensed Matter Physics, Institute of Physics, Chinese Academy of Sciences, Beijing* 100190, *China*

[3] *University of Chinese Academy of Sciences, Beijing* 100049, *China*

[4] *Key Laboratory of Quantum State Construction and Manipulation (Ministry of Education), Renmin University of China, Beijing* 100872, *China*

(Received 24 September 2025; revised manuscript received 7 January 2026; accepted manuscript online 9 January 2026)

A spin supersolid is characterized by the simultaneous breaking of lattice translation and continuous spin rotation symmetries. In this work, we study a spin-1 model with $U(2) \cong SU(2) \times U(1)/Z_2$ symmetry on the triangular lattice, and determine the phase diagram with a variational $\mathbb{C}P^2$ approach. We identify a novel supersolid phase which contains a 3-sublattice solid order and a superfluid order with spontaneous $SU(2)$-symmetry breaking. Unlike usual supersolid phases having only one Goldstone mode, the $SU(2)$-supersolid phase has two Goldstone modes. Another important feature of this supersolid is that the spin excitation spectrum has symmetry protected double degeneracy in the whole Brillouin zone. As by-products, several other ordered phases are obtained, including the ferromagnetic and the antiferromagnetic states breaking the $SU(2)$ symmetry, as well as genuine phases that completely break the $U(2)$ symmetry. Furthermore, the instabilities of $SU(3)$-flavor linear spin-wave theory are consistent with the phase boundaries between different ordered phases.

Keywords: supersolid, spontaneous symmetry broken, spin-wave, triangular lattice

PACS: 75.30.Kz, 75.40.Mg, 67.80.kb

DOI: 10.1088/1674-1056/ae3604 **CSTR:** 32038.14.CPB.ae3604

1. Introduction

The concept of supersolidity has attracted considerable interest in condensed matter physics since its proposal in 1970.[1] A supersolid is an exotic phase of matter characterized by the simultaneous coexistence of Bose–Einstein condensation (BEC) and density wave order, spontaneously breaking both the $U(1)$ particle number conservation symmetry and continuous translational symmetry. However, the existence of such a phase in continuum Bose gases remained controversial for many years.[2–4]

Later, it was proposed that the lattice version of the supersolid phase can indeed arise for hard-core bosons (bosons having infinite on-site repulsion) in the extended Hubbard model on frustrated lattices with nearest-neighbor interactions.[5] Since the hard core Boson model can be exactly mapped into a spin-1/2 XXZ system, the resultant supersolid phase is essentially a spin supersolid, namely, a magnetic phase with the emergence of spin-superfluid order (i.e., in-plane magnetic order) that simultaneously breaks the original lattice translation symmetry (characterized by enlarged unit cells). This scenario for realizing supersolids in hard-core bosons or spin systems was first illustrated via mean field theory[5] and later verified by a series of numerical studies.[6–17] The spin-supersolid order enriches the family of magnetic phases of matter and has attracted the interest of the experimental studies. Recently, progress has been made in the realization of the spin supersolid phases in the material $Na_2BaCo(PO_4)_2$.[18,19]

On the other hand, magnets carrying spin larger than $1/2$ can also support exotic phases of matter. For instance, many quantum phases exist in spin-1 systems, such as the Haldane chain[20–22] and general symmetry protected topological phases,[23–29] chiral spin liquids,[30–33] and so on. Like the mapping between spin-1/2 systems and hard-core bosons, a spin-1 magnet can also be considered as a bosonic system in which the hard-core constraint is relaxed to $0 \leq \langle n_i \rangle \leq 2$.[34–36] Since the 3-dimensional bosonic Hilbert space supports eight linearly independent Hermitian operators (other than the identity matrix), generally one should consider the three states of spin-1 as the basis carrying the fundamental representation of the $SU(3)$ group. Consequently, many classical orders can exist for spin-1 systems, including the magnetic dipole order, quadrupole order (also called spin nematic order),[37–41] and even $U(1)$ spin supersolid phases.[36,42,43]

In this work, we study a triangular lattice spin-1 model with $U(2)$ symmetry. Using a semiclassical approach, we obtain a supersolid phase which spontaneously breaks the

[†]Corresponding author. E-mail: liuzxphys@ruc.edu.cn

© 2026 Chinese Physical Society and IOP Publishing Ltd. All rights, including for text and data mining, AI training, and similar technologies, are reserved.

$SU(2) \subset U(2)$ symmetry as well as the lattice translation symmetry. This supersolid phase contains collinear 'antiferromagnetic' (AFM) order in the $SU(2)$ sector and two Goldstone modes. Besides, we find several other ordered phases, including a solid phase, a $SU(2)$-'ferromagnetic' (FM) phase, a $SU(2)$-120° 'antiferromagnetic' (AFM) phase, and other spin nematic phases which completely break the $U(2)$ symmetry. Furthermore the $SU(3)$ spin wave spectrum indicates that the instability of the 'magnons' agrees with the phase boundary of the semiclassical phase diagram.

The rest of the paper is organized as follows. In Section 2, we introduce the model and its symmetries as well as semi-calssical variational wave functions. The phase diagram, phase transitions and the properties of each phase are given in Section 3. In Section 4, the spin wave spectrum is provided, especially the magnon bands of the $SU(2)$ supersolid phase are shown to have symmetry protected double degeneracy. Section 5 is dedicated to summary and discussion.

2. Model and variational states

2.1. Spin-1 model with $U(2)$ symmetry

We start from the following SU(3) Heisenberg model which has the highest symmetry for spin-1 systems:

$$H_{\mathrm{su3}} = J_3 \sum_{\langle ij \rangle} \sum_{\alpha=1}^{8} \lambda_i^{\alpha} \lambda_j^{\alpha}, \tag{1}$$

where $\lambda^1, \ldots, \lambda^8$ are the eight Gell–Mann matrices which generate the $SU(3)$ group. Here we slightly modify the form of the Gell–Mann matrices λ^3 and λ^8 as

$$\lambda^3 = \begin{pmatrix} 1 & 0 & 0 \\ 0 & 0 & 0 \\ 0 & 0 & -1 \end{pmatrix}, \quad \lambda^8 = \frac{1}{\sqrt{3}} \begin{pmatrix} 1 & 0 & 0 \\ 0 & -2 & 0 \\ 0 & 0 & 1 \end{pmatrix},$$

and keep the rest ones unchanged:

$$\lambda^1 = \begin{pmatrix} 0 & 1 & 0 \\ 1 & 0 & 0 \\ 0 & 0 & 0 \end{pmatrix}, \quad \lambda^2 = \begin{pmatrix} 0 & -\mathrm{i} & 0 \\ \mathrm{i} & 0 & 0 \\ 0 & 0 & 0 \end{pmatrix},$$
$$\lambda^4 = \begin{pmatrix} 0 & 0 & 1 \\ 0 & 0 & 0 \\ 1 & 0 & 0 \end{pmatrix}, \quad \lambda^5 = \begin{pmatrix} 0 & 0 & -\mathrm{i} \\ 0 & 0 & 0 \\ \mathrm{i} & 0 & 0 \end{pmatrix},$$
$$\lambda^6 = \begin{pmatrix} 0 & 0 & 0 \\ 0 & 0 & 1 \\ 0 & 1 & 0 \end{pmatrix}, \quad \lambda^7 = \begin{pmatrix} 0 & 0 & 0 \\ 0 & 0 & -\mathrm{i} \\ 0 & \mathrm{i} & 0 \end{pmatrix}.$$

Notice that the nonzero entries of the generators λ_4, λ_5, λ_3, are essentially three Pauli matrices $\sigma^x, \sigma^y, \sigma^z$ within the subspace spanned by the first two bases $|1\rangle, |-1\rangle$ of the spin-1 Hilbert space, and generate an $SU(2)$ subgroup of $SU(3)$. Furthermore, since λ^8 commutes with the three generators $\lambda_3, \lambda_4, \lambda_5$, these four generators together generate the complete symmetry group $U(2) = SU(2) \times U(1)/Z_2$ of the 2-dimensional subspace spanned by $|1\rangle, |-1\rangle$, where the subgroup $U(1)$ is generated by λ^8 and the spin parity group $Z_2 = \{E, P_s\}$ is the common center of $SU(2)$ and $U(1)$ with the spin parity defined by

$$P_s = \mathrm{e}^{-\mathrm{i}\lambda^3 \pi} = \mathrm{e}^{-\mathrm{i}\lambda^4 \pi} = \mathrm{e}^{-\mathrm{i}\lambda^5 \pi} = (-1)^{S_z}.$$

Actually, the four operators of $U(2)$ can be expressed in forms of $S = 1$ spin operators as

$$\lambda^4 = S_x^2 - S_y^2, \quad \lambda^5 = S_{xy} = S_x S_y + S_y S_x,$$
$$\lambda^3 = S_z, \quad \lambda^8 = \frac{1}{\sqrt{3}}(3S_z^2 - 2).$$

Similarly, the rest generators can also be written in forms of spin operators as $\lambda^{1,6} = \frac{1}{\sqrt{2}}(S_x \pm S_{xz}), \lambda^{2,7} = \frac{1}{\sqrt{2}}(S_y \pm S_{yz})$.

The above $U(2)$ symmetry allows additional interactions, including the J_2 term in the $SU(2)$ sector,

$$H_{\mathrm{su2}} = J_2 \sum_{\langle ij \rangle} \sum_{m=3}^{5} \lambda_i^m \lambda_j^m, \tag{2}$$

and the λ_8-term in the $U(1)$ sector,

$$H_{\mathrm{u1}} = J_1 \sum_{\langle ij \rangle} \lambda_i^8 \lambda_j^8. \tag{3}$$

The model we will study in the present work is the sum of the three terms in Eqs. (1)–(3):

$$H = H_{\mathrm{u1}} + H_{\mathrm{su2}} + H_{\mathrm{su3}}. \tag{4}$$

We will only consider the 'anti-ferromagnetic' coupling with $J_1 > 0$, and will fix $J_3 = 1$ in the following discussion.

Besides the $U(2) \cong SU(2) \times U(1)/Z_2 \subset SU(3)$ symmetry,[41] the above model also preserves lattice translation symmetry, spatial inversion symmetry P, time reversal symmetry

$$T = \mathrm{e}^{-\mathrm{i}\frac{\lambda_5}{2}\pi} K = \mathrm{e}^{-\mathrm{i}\frac{S_{xy}}{2}\pi} K = \begin{pmatrix} & & -1 \\ & 1 & \\ 1 & & \end{pmatrix} K, \tag{5}$$

and D_6 point group symmetry, with

$$P^2 = 1, \quad T^2 = P_s = \mathrm{diag}(-1, 1, -1), \quad T^4 = 1$$
$$T\lambda^8 T^{-1} = \lambda^8, \quad T\lambda^{3,4,5} T^{-1} = -\lambda^{3,4,5},$$
$$T\lambda^{1,2} T^{-1} = \lambda^{6,7}, \quad T\lambda^{6,7} T^{-1} = -\lambda^{1,2}.$$

2.2. Semiclassical variational wave functions

Any state in the Hilbert space of a single spin-1 can be written as

$$|\boldsymbol{d}\rangle = d_+ |1\rangle + d_0 |0\rangle + d_- |-1\rangle, \tag{6}$$

where $|1\rangle, |0\rangle, |-1\rangle$ are the eigenstates of $\hat{S}^z$ with eigenvalues $1, 0, -1$, respectively. The coefficients d_+, d_0, d_- are complex

numbers subject to the normalization constraint $|d_+|^2+|d_0|^2+|d_-|^2=1$.

Since an overall phase shift does not yield a distinct physical state, the complete manifold of a spin-1 state is $SU(3)/U(2)\cong\mathbb{C}P^2$. A feasible parameterization scheme of this manifold is given by

$$d_+=\theta_2^{1/4}\theta_1^{1/2}\mathrm{e}^{\mathrm{i}\phi_1},\quad d_0=\theta_2^{1/4}\sqrt{1-\theta_1}\,\mathrm{e}^{\mathrm{i}\phi_2},$$
$$d_-=\sqrt{1-\theta_2^{1/2}},$$

where $0\le\theta_1,\theta_2\le1$ and $0\le\phi_1,\phi_2\le2\pi$ are $\mathbb{C}P^2$ parameters chosen from a uniform distribution.[44] Within this classical framework, we adopt a variational wave function for the spin-1 many-body state in a direct product form

$$|\Psi\rangle=\bigotimes_{i=1}^{N}|\boldsymbol{d}_i(\theta_{1i},\theta_{2i},\phi_{1i},\phi_{2i})\rangle. \tag{7}$$

This is so-called $\mathbb{C}P^2$ framework, as employed in Ref. [45]. Within this variational wavefunction, the expectation values of the order parameters on each site are $\langle\lambda_{4,i}\rangle=2\mathrm{Re}(d_{+i}^*d_{-i})$, $\langle\lambda_{5,i}\rangle=2\mathrm{Im}(d_{+i}^*d_{-i})$, $\langle\lambda_{3,i}\rangle=|d_{+i}|^2-|d_{-i}|^2$, $\langle\lambda_{8,i}\rangle=\frac{1}{\sqrt{3}}(1-3|d_{0i}|^2)$.

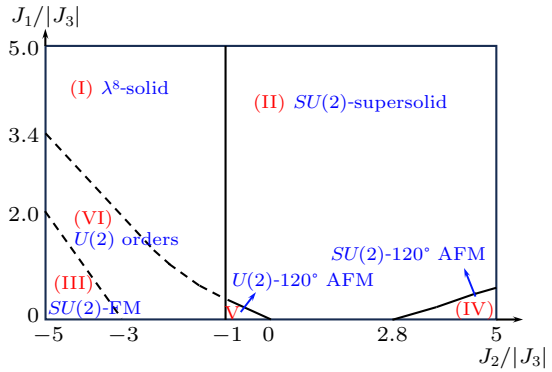


Fig. 1. The phase diagram of model (4) with $J_1>0$. There are totally six different phases: the λ^8-solid, the $SU(2)$-supersolid, the $SU(2)$-FM, the $SU(2)$-120° AFM, the $U(2)$-120° AFM, and the $U(2)$ orders. The solid line signifies the first-order transition, and the dashed line labels the second-order transition.

The energy of the trial state (7) is then given by

$$E=2J_3\sum_{\langle ij\rangle}\left(|d_{+i}^*d_{+j}+d_{0i}^*d_{0j}+d_{-i}^*d_{-j}|^2-\frac{2}{3}\right)$$
$$+J_2\sum_{\langle ij\rangle}\sum_{m=3}^{5}\langle\lambda_i^m\rangle\langle\lambda_j^m\rangle+J_1\sum_{\langle ij\rangle}\langle\lambda_i^8\rangle\langle\lambda_j^8\rangle. \tag{8}$$

The trial state (7) generally contains long-range order. Assuming that the unit cell contains n_Λ sites,[46,47] then the variational wave function can also be written as

$$|\Psi\rangle=\prod_{j=1}^{n_\Lambda}\prod_{i\in\Lambda_j}|\boldsymbol{d}_j\rangle_i, \tag{9}$$

where i is a site index, Λ_j denotes the set of sites belonging to the j-th sublattice, and the on-site wave function is assumed to be identical for all spins within the same sublattice (i.e., $|\boldsymbol{d}_j\rangle_{i_1}=|\boldsymbol{d}_j\rangle_{i_2}=\cdots$). Thus, the task of finding the ground state reduces to optimizing the energy functional (8) with respect to only $4n_\Lambda$ variables. It turns out that the lowest energy trial wave functions satisfy $n_\Lambda\le3$ according to our variational calculations. The final results are shown in the phase diagram Fig. 1, and the details will be discussed in the following sections.

3. Superfluids, solids and supersolids

3.1. Static structure factors and phase diagram

We use the static structure factor to characterize the long-range correlations of the trial wave functions. Among the eight generators, λ^8 and λ^3, λ^4, λ^5 are of importance since they generate the $U(2)$ symmetry group of Hamiltonian (4). Defining the vector $\boldsymbol{\lambda}^{\mathrm{su2}}=\lambda^4\boldsymbol{e}_x+\lambda^5\boldsymbol{e}_y+\lambda^3\boldsymbol{e}_z$ (where $\boldsymbol{e}_x,\boldsymbol{e}_y,\boldsymbol{e}_z$ are unit vectors), the static structure factors (SSFs) are given by

$$S_{\mathrm{su2}}(\boldsymbol{q})=\frac{1}{N}\sum_{i,\boldsymbol{\delta}}\langle\boldsymbol{\lambda}_i^{\mathrm{su2}}\cdot\boldsymbol{\lambda}_{i+\boldsymbol{\delta}}^{\mathrm{su2}}\rangle\,\mathrm{e}^{-\mathrm{i}\boldsymbol{q}\cdot\boldsymbol{\delta}},$$
$$S_8(\boldsymbol{q})=\frac{1}{N}\sum_{i,\boldsymbol{\delta}}\langle\lambda_i^8\lambda_{i+\boldsymbol{\delta}}^8\rangle\,\mathrm{e}^{-\mathrm{i}\boldsymbol{q}\cdot\boldsymbol{\delta}}. \tag{10}$$

We performed variational computation for the parameter region $-5\le J_2\le5, 0\le J_1\le5$ using Eq. (9) as the variational ansatz, where the unit cell contains up to $n_\Lambda=6\times6$ lattice sites. Actually, the unit cell of all obtained ground states contains only $n_\Lambda\le3$ sites, hence we can use the SSF at $\boldsymbol{q}=\Gamma,K$, as shown in Figs. 2(a)–2(d), to distinguish different phases. As shown in the phase diagram in Fig. 1, six phases are obtained and labeled by I–VI. The patterns of various orders in these phases are illustrated in Fig. 3 by the expectation value of $\langle\boldsymbol{\lambda}^{\mathrm{su2}}\rangle$ and $\langle\lambda^8\rangle$ on each sublattice, where $\langle\boldsymbol{\lambda}^{\mathrm{su2}}\rangle$ is plotted as a three-dimensional vector, and $\langle\lambda^8\rangle$ is exhibited as a solid dot on each site with the radius representing the amplitude and the red/blue color denoting the positive/negative sign.

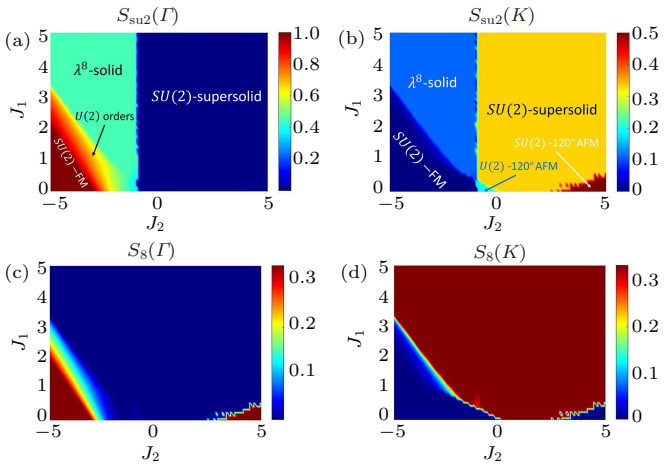


Fig. 2. Distributions of the static structure factor (SSF) at the Γ and K points for different parameters. (a) $S_{\mathrm{su2}}(\Gamma)$. (b) $S_{\mathrm{su2}}(K)$. (c) $S_8(\Gamma)$. (d) $S_8(K)$.

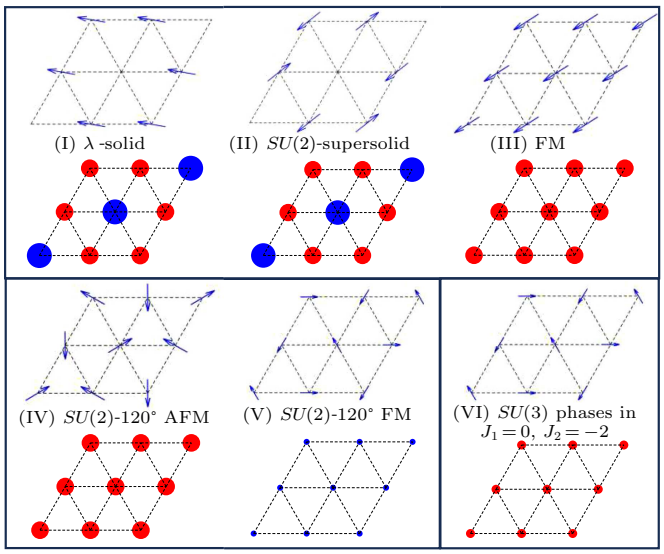


Fig. 3. Distribution of $\langle \boldsymbol{\lambda}^{\mathrm{su2}} \rangle$ and λ^8 on the sublattices for the five order phases (I)–(VI) identified in Fig. 2. The $\langle \lambda^3 \rangle$ components of $\langle \boldsymbol{\lambda}^{\mathrm{su2}} \rangle$ are ommitted for clarity. The value of $\langle \lambda^8 \rangle$ is indicated by a solid dot on each site, with the radius representing the amplitude and red/blue color denoting the positive/negative sign. For the phase (VI), only the configuration at $J_1 = 0, J_2 = -2$ has been exhibited.

3.2. Configuration of each phase

Phase-I is characterized by the solid order of $\langle \lambda^8 \rangle$ and exhibits a three-sublattice structure $(A,B,C) = (2\lambda, -\lambda, -\lambda)$. This phase is analogous to the solid phase on the triangular lattice in hard-core boson systems[9] and spin systems.[48] Hence the SSF $S_8(\boldsymbol{q})$ exhibits a peak at the K point. On the other hand, the magnitude of $\langle \boldsymbol{\lambda}^{\mathrm{su2}} \rangle$ is suppressed on the A-sublattice where λ^8 has a larger value. On the other two sublattices B and C, the value of $\langle \boldsymbol{\lambda}^{\mathrm{su2}} \rangle$ is 'ferromagnetic' and forms a hexagonal superlattice. The non-zero net value of $\langle \boldsymbol{\lambda}^{\mathrm{su2}} \rangle$ in the unit cell induces an additional signal of the static structure factor at the Γ point. Although the 'ferromagnetic' order $\langle \boldsymbol{\lambda}^{\mathrm{su2}} \rangle$ breaks the $SU(2)$ symmetry, the $SU(3)$ linear spin-wave dispersion is quadratic (see Fig. 6(a)) and cannot be considered as a 'superfluid'. Hence we term phase-I as a λ^8-solid phase.

It should be noticed that the $SU(2)$ group is generated by $\lambda^{3,4,5}$, where λ^3 is a magnetic dipole operator while $\lambda^{4,5}$ are quadrupole operators. Since the 'ferromagnetic' order $\langle \boldsymbol{\lambda}^{\mathrm{su2}} \rangle$ spontaneously breaks the $SU(2)$ symmetry, the resulting state generally contains coexisting magnetic dipole-order and quadrupole-order. The same situation also holds for all the other phases.

Phase-II is a very robust phase which contains a large volume in the phase diagram. It is also a solid phase of $\langle \lambda^8 \rangle$ with a three-sublattice structure $(A,B,C) = (2\lambda, -\lambda, -\lambda)$. Furthermore, the value of $\langle \boldsymbol{\lambda}^{\mathrm{su2}} \rangle$ in the $SU(2)$ sector also vanishes on the A-sublattice. The difference is that the configuration of $\langle \boldsymbol{\lambda}^{\mathrm{su2}} \rangle$ forms a Neel-type AFM order on the B- and C-sublattices . Hence the SSF S_{su2} exhibits a peak at the K point. This structure is analogous to the 'Y-phase' in the spin-1/2 systems.[14,18] The collinear $\langle \boldsymbol{\lambda}^{\mathrm{su2}} \rangle$-magnetic order breaks the $SU(2)$ symmetry, and keep the lattice periodicity of the $\langle \lambda^8 \rangle$ order. Furthermore, the linear spin wave dispersion of the AFM phase is linear, indicating that it is indeed a 'spin superfluid phase' which spontaneously breaks the $SU(2)$ symmetry to $U(1)$ (such that the total symmetry group reduces to $U(1) \times U(1)/Z_2$ with the first $U(1)$ generated by λ^8). Considering the coexistence of the solid order of $\langle \lambda^8 \rangle$ and the superfluid order of $\langle \boldsymbol{\lambda}^{\mathrm{su2}} \rangle$, phase-II can be termed a $SU(2)$-supersolid phase which has two Goldstone modes (see Fig. 7(b)). It is different from the supersolid phase in literature, which only breaks $U(1)$ spin rotation symmetry and contains only one Goldstone mode.

Furthermore, the $SU(2)$ symmetry breaking only occurs at zero temperature. The finite temperature KT transition, which appears in $U(1)$-supersolid phase, is likely to be absent just as in the 2-dimensional classical Heisenberg model with $SO(3)$ symmetry.[49] Nevertheless, a weak anisotropy in the $SU(2)$ sector can give rise to a KT phase at finite temperatures.

Phase-III is a uniform phase that does not break translation symmetry. In this phase, the distributions of $\langle \lambda^8 \rangle$ and $\langle \boldsymbol{\lambda}^{\mathrm{su2}} \rangle$ are both 'ferromagnetic' (FM), and only the $SU(2)$ symmetry is broken. The SSFs only exhibit peaks at the Γ point. Hence phase-III is called an $SU(2)$-FM phase.

Phase-IV is characterized by the 120°-AFM order of $\langle \boldsymbol{\lambda}^{\mathrm{su2}} \rangle$ which exhibits a 3-sublattice structure. However, no solid order of $\langle \lambda^8 \rangle$ is observed. It is analogous to the umbrella state found in spin-1/2 systems.[14] Therefore, this phase is not considered a supersolid, but rather an $SU(2)$-120°AFM phase. Since the $SU(2)$ symmetry is completely broken in the 120° AFM order, the spin wave dispersion contains three Goldstone modes (see Fig. 7(a)).

Table 1. Magnitudes of $\lambda^{3,4,5,8}$ and $\lambda^{1,2,6,7}$ for phase (IV) $SU(2)$-AFM, and (V) $U(2)$-AFM. The parameters are $J_2 = 5$, $J_1 = 0$ for $SU(2)$-AFM and $J_2 = -0.5$, $J_1 = 0$ for $U(2)$-AFM. Since the values are identical across all three sublattices for each phase, only the value for a single sublattice is listed.

	$\sum_{m=3,4,5,8} \langle \lambda^m \rangle^2$	$\sum_{m=1,2,6,7} \langle \lambda^m \rangle^2$
$SU(2)$-AFM	1.33	0
$U(2)$-AFM	0.4026	0.9307

Phase-V also contains the 120° AFM order for $\langle \boldsymbol{\lambda}^{\mathrm{su2}} \rangle$. But in this phase the value of $\langle \lambda^8 \rangle$ is suppressed to nearly zero on all sublattices. We further compare the quantities $\sum_{m=3,4,5,8} \langle \lambda^m \rangle^2$ and $\sum_{m=1,2,6,7} \langle \lambda^m \rangle^2$ in phase-IV ($J_2 = 5, J_1 = 0$) and phase-V ($J_2 = -0.5, J_1 = 0$). We find that for each phase, these two values are equal on all three sublattices. However, as summarized in Table 1, the value of $\langle \lambda^{1,2,6,7} \rangle$ is zero in phases I–IV (namely, all the orders only break the $SU(2)$ symmetry while preserving the $U(1)$ symmetry). In contrast, in phase-V (and in region-VI discussed below), the value of

$\sum_{m=1,2,6,7}\langle\lambda^m\rangle^2$ is significantly large, indicating that the order involves all eight generators of the $SU(3)$ group with complete breaking of the $U(2)$ symmetry. We therefore refer to phase-V as the $U(2)$-AFM phase.

The region-VI is sandwiched between the FM and the λ^8-solid and the value of $\sum_{m=1,2,6,7}\langle\lambda^m\rangle^2$ is also finite in this region. Actually, the region-VI contains more than one phase. For instance, a λ^8-solid-like phase emerges in the parameter region close to λ^8-solid phase (for instance, $J_2=-5, J_1=3.3$). The difference between the two phases is that $\langle\boldsymbol{\lambda}^{\mathrm{su2}}\rangle$ is zero in the A-sublattice in the λ^8-solid phase but nonzero (but small) in the λ^8-solid-like phase. On the other hand, in the parameter region between the FM (phase-III) and the $U(2)$-AFM (phase-V) (for instance, $J_2=-2.5, J_1=0$), a $U(2)$-FM-like phase emerges. The difference with the $SU(2)$-FM phase is that in the $U(2)$-FM-like phase, the weight of $\langle\lambda^8\rangle$ is suppressed and shifted to the remaining components $\langle\lambda^{1,2,6,7}\rangle$ (see Fig. 3(VI) for illustration). Generally, in region-VI the $U(2)$ generators are not sufficient to describe the orders any more. We will not go into many details in this region.

Finally, the stability of the $U(2)$ ordered phases is determined by $|J_3|$, the amplitude of the $SU(3)$-symmetric interaction H_{su3}. With the decrease of $|J_3|$, the extent of phase-V and region-VI reduces. Especially, when $J_3=0$, the phase boundary between the λ^8-solid and $SU(3)$ phases becomes a straight line given by $|J_1|=|J_2|$, and both phase-V and region-VI completely disappear (see Fig. 4).

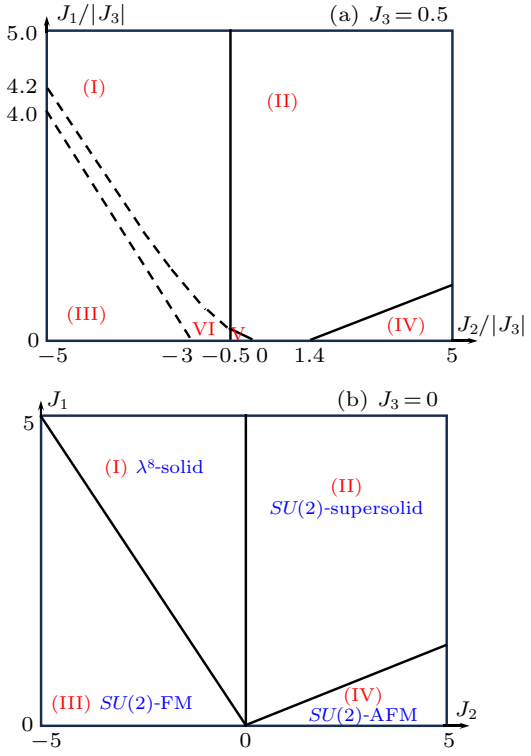


Fig. 4. Variational phase diagram for the $U(2)$ model with different $SU(3)$ background coupling strengths. (a) $J_3=-0.5$. (b) $J_3=0$.

3.3. Phase transitions

To illustrate the phase transitions, we consider a one-parameter curve $J_2=r\cos\theta, J_1=r\sin\theta$ with $r=5$ and $0\le\theta\le\pi$. This curve covers five different phases, along which two first-order phase transitions and two continuous phase transitions are observed (see Fig. 5).

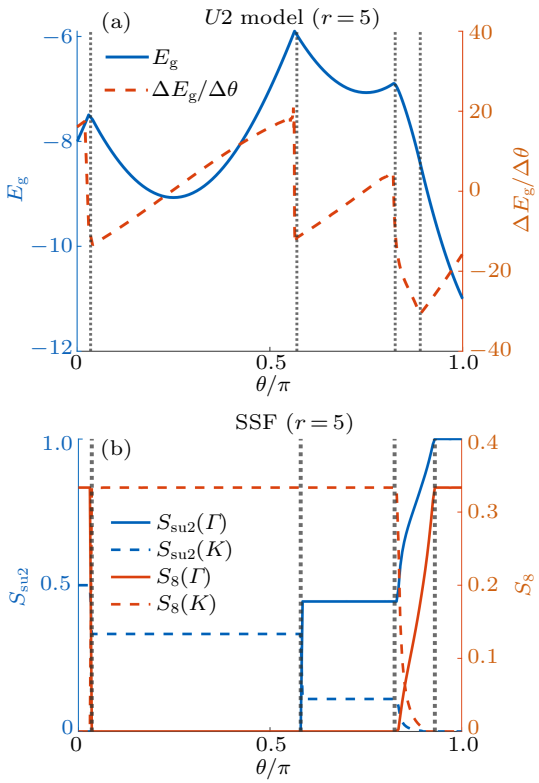


Fig. 5. Variational computation results for different parameter $\theta=\arctan J_1/J_2$ with $r=\sqrt{J_1^2+J_2^2}=5$. (a) Energy of the variational ground state. The blue solid line represents the calculation results. The red scatter points are the first-order difference of energy. (b) Four SSF curves of the variational ground state. The solid line represents the value at the Γ point while the dashed line represents the value at the K point. The blue curves represent the results of $S_{\mathrm{su2}}(\boldsymbol{q})$, while the red curves represent the results of $S_8(\boldsymbol{q})$.

The SSFs and the first order derivative of the energy curve $\partial E/\partial\theta$ exhibit discontinuous jumps at $\theta/\pi=0.035, 0.58$, corresponding to the first-order phase transitions between phase-IV and phase-II, and between phase-II and phase-I, respectively. In contrast, the continuous change of SSFs and $\partial E/\partial\theta$ at $\theta/\pi=0.825, 0.93$, suggests a second-order transition between phase-I and region-VI, and between region-VI and phase-III, respectively.

Within the interval $0.825<\theta/\pi<0.93$, all four SSF curves are non-zero and continuous, implying that the $SU(3)$-region-(VI) plays the role of a 'transitional phase'. When setting $J_3=0$, with the disappearance of the $SU(3)$-region-(VI), the direct transition between λ^8-Solid and FM becomes first-order.

The transitions from phase-V to its neighboring phases (i.e., phase-II and region-VI), which are not covered by the above curve with $r=5$ and $0\le\theta\le\pi$, are both first order.

4. $SU(3)$ spin-wave

To verify the stability of the classically ordered phases, we calculate the $SU(3)$ linear spin-wave[50,51] in various regions of the phase diagram. Our results indicate that the edges for the spin-wave instabilities are in good consistency with the phase boundaries from the variational calculation, which indicates the validity of the semi-classical phase diagram.

4.1. λ^8-solid (phase-I)

We consider a typical λ^8-solid state with the configuration $|\psi_A\rangle = |\psi_B\rangle = |1\rangle, |\psi_C\rangle = |0\rangle$. The results of the $SU(3)$ spin-wave calculation for this state at several parameter points are shown in Fig. 6. The spectra E_1, E_5 are always gapless at the Γ point and exhibit a quadratic dispersion relation, which is characteristic of ferromagnetism. With the decrease of J_2, the bandwidths of E_1 and E_5 become narrow, eventually turning completely flat and degenerate at zero energy when $J_2 = -1.0$. If the magnitude of the antiferromagnetic J_2 is further reduced (i.e., $J_2 > -1$), these two bands develop a negative quadratic form, indicating an instability and a phase transition from the ferromagnetic-like state to an antiferromagnetic state, as discussed previously.

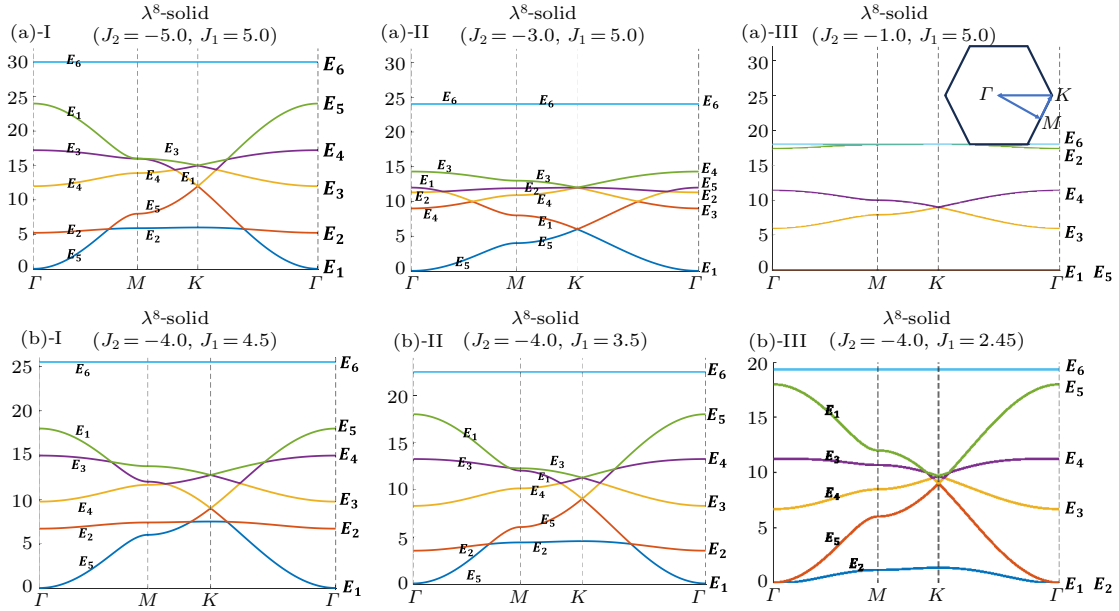


Fig. 6. Spin wave spectrum for a typical λ^8-solid state. The magnon branch index E_i is marked on the curves. (a) Spectra for $J_1 = 5.0$ and several values of J_2. (b) Spectra for $J_2 = -4.0$ and several values of J_1. The inset of (a-III) shows the path taken in the first magnetic Brillouin zone for these calculations.

On the other hand, if the strength of J_2 is fixed while parameter J_1 is reduced, the overall structure of the spectra remains largely unchanged. However, the band E_2 shifts downward and eventually closes its gap at the Γ point near the transition. If the antiferromagnetic coupling J_1 is weakened further, E_2 develops negative excitation energies, signaling the instability of the FM order.

4.2. $SU(2)$-supersolid (phase-II)

Next, we calculate the spin-wave spectrum for the $SU(2)$-supersolid state (phase-II). Since the $SU(2)$ symmetry is spontaneously broken, the resulting $SU(2)$ order can be oriented along arbitrary direction. Without loss of generality, we assume that the $SU(2)$ order is carried by λ^3. Notice that all of $\lambda^{3,4,5}$ reverse their sign under the action of T, the three generators are equivalent from the symmetry point of view. Then the classical ground state reads $|\psi_A\rangle = |1\rangle, |\psi_B\rangle = |-1\rangle, |\psi_C\rangle = |0\rangle$ respectively on the three sublattices.

Interestingly, the spin wave spectrum is doubly degenerate everywhere in the Brillouin zone (BZ). Hence only three distinct magnon dispersions are observed. Among the six magnon bands, the modes E_1, E_2 are gapless at the Γ point and exhibit linear dispersion. This is a signature of the existence of spin superfluid order.

Actually, the double degeneracy of the magnon spectrum is not accidental. In the ground state of the $SU(2)$ supersolid phase, the inversion symmetry P and time reversal symmetry T in Eq. (5) are broken, but the combined symmetry PT with $(PT)^4 = 1$ is preserved (where the inversion center of PT is located on the site of the C sub-lattice). Furthermore, the $SU(2)$ symmetry generated by $\lambda^{3,4,5}$ is broken down to $U(1) = \{e^{-i\lambda^3\theta}; 0 \le \theta < 2\pi\}$ generated by $\lambda^3 = S_z$. Here we ignore the $U(1)$ symmetry generated by λ^8 since it does not contribute to the degeneracy. Since PT anti-commutes with λ_3, the group formed by the remaining symmetries reads $G = U(1) \times Z_4^{PT}/Z_2$ with $Z_4^{PT} = \{E, PT, P_s, P_sPT\}, (PT)^2 = P_s, Z_2 = \{E, P_s\}$, where $P_s = e^{-i\lambda^3\pi} = e^{-i\lambda^4\pi} = e^{-i\lambda^5\pi}$ is the spin parity. Noticing that both the unitary elements $e^{-i\lambda^3\theta}$ and the anti-unitary element PT do not change the lattice momentum, the spin-wave Hamiltonian at each $\boldsymbol{k}$ point has the full

symmetry $G = U(1) \times Z_4^{PT}/Z_2$. Furthermore, the magnon creation operators carry the 2-dimensional irreducible representations (irreps) in Table 2 (see Appendix B for details), which yields the double degeneracy of the magnon bands throughout the BZ. This degeneracy can be lifted by perturbations that break the G symmetry. For example, by applying a magnetic field coupling to λ^3, two of the three degenerate bands including the one containing two Goldstone modes, undergo energy splitting (see Fig. 7(c)). The splittings of the energy bands of the spin excitations are observable in experiments, and can be used to distinguish from the $U(1)$-supersolid phase.

It is worth mentioning that the two Goldstone modes created by $\lambda^4 \pm \mathrm{i}\lambda^5$ are not usual 'magnons', because they carry quantum numbers ± 2 of S_z, similar to the case in spin-1 XXZ model.[43] For this reason, the gapless Goldstone modes cannot be detected by neutron scattering experiment. However, if the $\boldsymbol{\lambda}^{\mathrm{su2}}$ is oriented along different directions, then the Goldstone mode can contain both $S_z = \pm 2$ and $S_z = 0$ components, then can couple to neutron spin. On the other hand, by adopting the original $\lambda^{3,8}$ and redefining the $SU(2)$ symmetry of the model as generated by $\lambda^{1,2,3}$ (see Appendix C), then the Goldstone modes of the $SU(2)$-supersolid will generally be detectable in neutron scattering experiments.

With J_1 fixed at 4.0 (a strong antiferromagnetic coupling), we gradually decrease J_2 towards the ferromagnetic value $J_2 = -1.0$ (see Fig. 7(a)). The maximum excitation energy of magnons E_1 and E_2 decreases, eventually reaching zero across the entire first magnetic BZ. A further increase in the ferromagnetic strength of J_2 (i.e., more negative value) results in globally negative excitation energies for E_1, E_2, indicating an instability and a phase transition. This behavior of the spectrum upon varying J_2 is similar to that observed in the λ^8-solid case, where bands E_1, E_5 become flat at $J_2 = -1$ and exhibit trends analogous to bands E_1 and E_2 here.

Next, we fix J_2 at a small ferromagnetic value $J_2 = -0.5$ and gradually reduce J_1 (see Fig. 7(b)). The shape of the dispersion curves for E_1, E_2 remains unchanged, but the energies of E_3, E_4, E_5, E_6 are shifted downward. At $J_1 = 0.18$, which corresponds to the transition point between the $SU(2)$-supersolid and $SU(3)$-120° AFM phases, the gap of bands E_3 and E_4 closes. For values of J_1 below this critical point, parts of the spectrum develop imaginary excitation energies, indicating that the classically-ordered $SU(2)$-supersolid state becomes unstable.

Table 2. A 2-dimensional irreducible representation of the group $G = U(1) \times Z_4^{PT}/Z_2$ carried by magnon creation operators.

	$\mathrm{e}^{-\mathrm{i}\lambda^3\theta}$	PT	Bases
irrep-(1)	$\begin{pmatrix} \mathrm{e}^{-\mathrm{i}\theta} & \\ & \mathrm{e}^{\mathrm{i}\theta} \end{pmatrix}$	$\begin{pmatrix} -1 & \\ 1 & \end{pmatrix} K$	$[(\lambda^1 + \mathrm{i}\lambda^2), (\lambda^6 - \mathrm{i}\lambda^7)]$, $[(\lambda^6 + \mathrm{i}\lambda^7), -(\lambda^1 - \mathrm{i}\lambda^2)]$.
irrep-(2)	$\begin{pmatrix} \mathrm{e}^{-2\mathrm{i}\theta} & \\ & \mathrm{e}^{2\mathrm{i}\theta} \end{pmatrix}$	$\begin{pmatrix} & 1 \\ 1 & \end{pmatrix} K$	$[(\lambda^4 + \mathrm{i}\lambda^5), -(\lambda^4 - \mathrm{i}\lambda^5)]$.

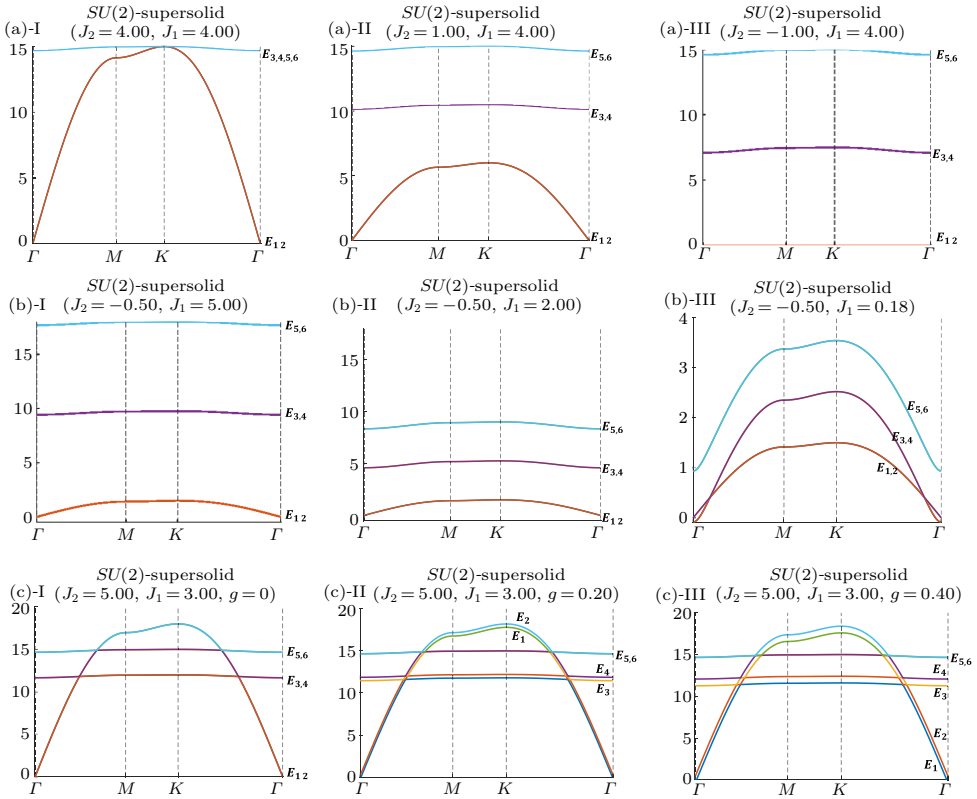


Fig. 7. Spin-wave spectra for the $SU(2)$-supersolid state. The magnon branch index E_i is marked on the curves. The calculation path is the same as Fig. 6. Different series show results for different parameter settings. (a) Spectra for $J_1 = 0.4$ and several values of J_2 with $SU(2)$-supersolid as reference state. (b) Spectra for $J_2 = -0.5$ and several values of J_1 with $SU(2)$-supersolid as reference state. (c) Spectra for adding magnetic field coupling with $\lambda^3 = S^z$. Here we denote g as coupling strength, i.e., the model Hamiltonian has been modified as $H' = H + g\sum_i \lambda_i^3$.

Finally, when $J_2 = J_3$, the bands $E_{3,4}$ will be degenerate with the bands $E_{5,6}$. If one further tunes $J_2 = J_3 = 0$ such that the model is fully $SU(3)$ symmetric, then all six bands become completely degenerate in the whole Brillouin zone. This result is consistent with a previous study of $SU(3)$ Heisenberg model in Ref. [52], where six-fold degeneracy of the excitation spectrum is observed in the reduced Brillouin zone.

4.3. $SU(2)$-FM (phase-III)

Then we calculate the spin-wave spectrum in the FM phase (phase-III). The FM order contains only one sublattice, hence two branches of magnons are expected from $SU(3)$ linear spin wave theory. Starting from the classical ground state $|\psi_i\rangle = |1\rangle$, one obtains the following two magnon bands with dispersion

$$E_1(\boldsymbol{k}) = -2(J_3+J_2)(6-\gamma_{\boldsymbol{k}}),$$
$$E_2(\boldsymbol{k}) = -2[3(J_1+J_2)+J_3(6-\gamma_{\boldsymbol{k}})].$$

Here $\gamma_{\boldsymbol{k}} = \sum_{\boldsymbol{\delta}\in nn} \mathrm{e}^{-\mathrm{i}\boldsymbol{k}\cdot\boldsymbol{\delta}}$ is the structural form factor. Parameterizing momentum as $\boldsymbol{k} = k_1\boldsymbol{b}_1 + k_2\boldsymbol{b}_2$ (where $\boldsymbol{b}_1, \boldsymbol{b}_2$ are the reciprocal lattice vectors), then one obtains

$$\gamma_{\boldsymbol{k}} = 2(\cos 2\pi k_1 + \cos 2\pi k_2 + \cos 2\pi(k_1 - k_2)). \tag{11}$$

Notice that the factor $(6-\gamma_k) \geq 0$ is always valid. $(6-\gamma_k)$ equals 0 at the Γ point and has a quadratic dispersion at small moments. Furthermore, the magnon excitations must take non-negative energy, which requires that $E_1(\boldsymbol{k}) \geq 0$, namely,

$$J_3 + J_2 < 0. \tag{12}$$

Violating of the above condition means the instability of the FM order. When Eq. (12) is satisfied, then $E_1(\boldsymbol{k})$ is gapless at the Γ point and has quadratic magnon dispersion, which is the signature feature of the FM order.

On the other hand, the other band $E_2(\boldsymbol{k})$ is generally gapped, hence $E_2(\boldsymbol{k}) > 0$ should be valid in the whole Brillouin zone. It requires that $3(J_1+J_2)+J_3(6-\gamma_{\boldsymbol{k}}) < 0$, namely, $J_1 + J_2 < \frac{J_3}{3}(\gamma_k - 6)$ for any $\boldsymbol{k}$. Since $(\gamma_k - 6)$ takes its minimum value -3 at the K point, one should have

$$J_1 + J_2 < -3J_3. \tag{13}$$

At the parameter line $J_1 + J_2 = -3J_3$, the $E_2(\boldsymbol{k})$ band becomes gapless at the K point, namely, $E_2(K) = 0$. This indicates that the magnons will undergo BEC. The condensation of magnons with momentum K indicates a phase transition to another ordered phase with three sublattices.

Especially, if $J_3 = 0$, the phase transition line becomes $J_1 = -J_2$. These results are consistent with our earlier variational calculations.

4.4. $SU(2)$-120° AFM (phase-IV)

We performed a variational calculation for the parameters $J_2 = 5.0, J_1 = 0.0$ to obtain the components of $|\psi_A\rangle, |\psi_B\rangle, |\psi_C\rangle$ in the S^z basis. This state served as the reference state for the spin-wave calculation.

The six magnon spectra can be classified into two sets. The first set consists of three gapless modes (E_1, E_2, E_3) whose gaps close at the Γ point. They exhibit a linear dispersion near the Γ point, which is a typical signature of antiferromagnetism. Those three branches of linearly dispersive gapless magnons correspond to the three Goldstone modes arising from the complete breaking of the $SU(2)$ symmetry.

The other three magnons are gapped across most of the $SU(2)$-120° AFM phase region. Their excitation energies shift overall with changes in J_1 and J_2. As shown in Fig. 8(a), the energies of these modes decrease as the antiferromagnetic coupling J_1 strengthens, eventually becoming gapless at the phase boundary, indicating a phase transition.

4.5. $U(2)$-AFM (phase-V)

Finally, we calculate the spin-wave spectrum for the $U(2)$-AFM state (phase-V) at $J_2 = -0.5$, $J_1 = 0.1$ (see Fig. 8(b)), with the reference configuration chosen from the results of variational calculation. Since the nonzero values of $\langle\lambda^{1,2,6,7}\rangle$ completely break the $U(2)$ symmetry, the spin-wave dispersion contains four branches of gapless Goldstone modes and the rest two are gapped.

If we change the parameters to another point within the $SU(3)$-AFM region but keep the reference configuration unchanged, imaginary spectra will appear near the Γ point, which implies quantum fluctuations are strong in this phase.

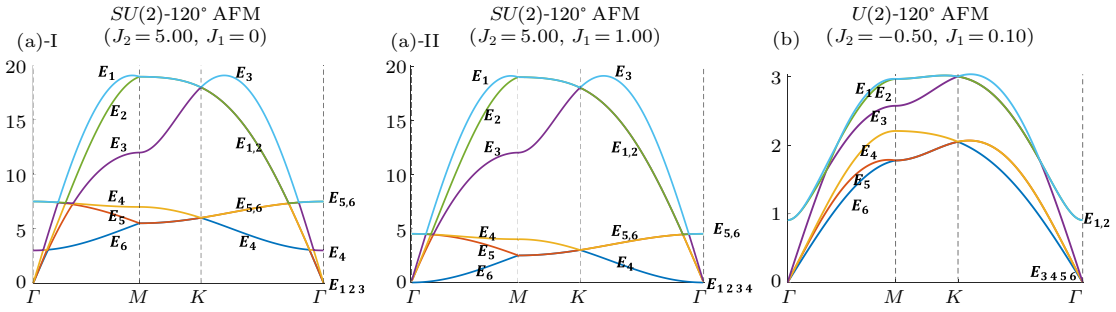


Fig. 8. Spin-wave spectra for the $SU(2)$-120° AFM state, $U(2)$-120° AFM state. The magnon branch index E_i is marked on the curves. The calculation path is the same as Fig. 6. Different series show results for different settings. (a) Spectra for $J_2 = 5.0$ and two values of J_1 with $SU(2)$-120° AFM as reference state. (b) Spectra for $J_2 = -0.5, J_1 = 0.1$ with $U(2)$-120° AFM as reference state.

5. Discussion and conclusion

In summary, we studied a $U(2) = SU(2) \times U(1)/Z_2$ symmetric spin-1 model on the triangular lattice. By employing a variational calculation within a classical $\mathbb{C}P^2$ ansatz, we determined a rich phase diagram that contains various long-range ordered phases. The most significant finding of this work is the identification of a robust $SU(2)$-supersolid phase. In this phase, the system spontaneously breaks both the spin $SU(2)$ symmetry — via a non-collinear magnetic order of $\boldsymbol{\lambda}^{\mathrm{su2}}$ — and the lattice translation symmetry — via a solid order parameter λ^8 with a 3-sublattice $(2,-1,-1)$ pattern. This represents a direct generalization of the supersolid phenomenon to a higher spin context with a more complex broken symmetry group. The stability of this classically ordered state and its characteristic excitation spectrum, including intriguing degeneracies, were further validated by $SU(3)$ linear spin-wave theory.

Beyond the supersolid, our study unveils a few other phases. These include conventional FM or 120°-AFM phases within the $SU(2)$ sector, where translational symmetry remains intact or is broken by the magnetic order itself. Notably, in regions where J_1, J_2 are weak, the non-zero value of $\sum_{m=1,2,6,7}\langle\lambda^m\rangle^2$ implies a more exotic ordered state which completely breaks the $U(2)$ symmetry. The nature of these phases warrants further investigation.

Our work establishes the designed $U(2)$ model as a fertile ground for exploring complex magnetic orders and multiple symmetry breaking in spin-1 systems. The natural next step involves comparing these classical and spin-wave results with fully quantum-mechanical numerical simulations to assess the impact of quantum fluctuations. Furthermore, it would be intriguing to explore the potential realization of these phases in realistic magnetic compounds or quantum simulators featuring spin-1 moments on triangular lattices.

Appendix A: Details of spin wave calculations

A1. Spin wave of FM state

Let $|1\rangle, |0\rangle, |-1\rangle$ denote the eigenstates in the $\hat{S}^z$ basis, in which Gell-Mann matrices take their standard form. Without loss of generality, the FM state $|FM\rangle$ can be chosen as $|FM\rangle = \prod_i |1\rangle_i$. Introducing Schwinger Boson via the mapping $\hat{b}_1|\mathrm{vac}\rangle \cong |1\rangle, \hat{b}_0|\mathrm{vac}\rangle \cong |0\rangle, \hat{b}_{-1}|\mathrm{vac}\rangle \cong |-1\rangle$,[53] the spin-wave theory treatment assumes the condensation of the $\hat{b}_1$ boson, while $\hat{b}_0, \hat{b}_{-1}$ become the Holstein–Primakoff (HP) bosons. The Gell–Mann matrices can then be rewritten in terms of Schwinger bosons. The operator $\hat{b}_1$ is approximated as

$$\hat{b}_1^\dagger \approx \hat{b}_1 \approx \sqrt{1 - \hat{b}_0^\dagger \hat{b}_0 - \hat{b}_{-1}^\dagger \hat{b}_{-1}} \tag{A1}$$

reflecting the constraint on the total boson number per site. Within the linear spin-wave approximation, the single operators $\hat{b}_1, \hat{b}_1^\dagger$ are replaced by 1, while their product is substituded using the number constraint

$$b_1^\dagger \hat{b}_1 = 1 - \hat{b}_0^\dagger \hat{b}_0 - \hat{b}_{-1}^\dagger \hat{b}_{-1}. \tag{A2}$$

Expanding the Hamiltonian and retaining terms up to quadratic order in the HP boson operators yields the general form

$$\begin{aligned}\hat{H} = &\sum_{\langle ij\rangle} (T_{\alpha\beta} \hat{b}_{i\alpha}^\dagger \hat{b}_{j\beta} + \Delta_{\alpha\beta} \hat{b}_{i\alpha}^\dagger \hat{b}_{j\beta}^\dagger + \mathrm{h.c.}) \\ &+ 12 \sum_i V_{\alpha\beta} \hat{b}_{i\alpha}^\dagger \hat{b}_{i\beta} + E_0,\end{aligned} \tag{A3}$$

where the indices α, β run over the two flavors of HP bosons (0 and -1), and the matrices are defined by

$$\begin{cases} V_{\alpha\beta} = \sum_{m=1}^8 J^m \lambda_{00}^m (\lambda_{\alpha\beta}^m - \lambda_{00}^m \delta_{\alpha\beta}), \\ T_{\alpha\beta} = \sum_{m=1}^8 J^m \lambda_{\alpha 0}^m \lambda_{0\beta}^m, \\ \Delta_{\alpha\beta} = \sum_{m=1}^8 J^m \lambda_{\alpha 0}^m \lambda_{\beta 0}^m. \end{cases} \tag{A4}$$

For our model Hamiltonian, the coupling strengths J^m are assigned as

$$J^m = \begin{cases} J_2 + J_3, & m = 3,4,5, \\ J_3, & m = 1,2,6,7, \\ J_1 + J_3, & m = 8. \end{cases} \tag{A5}$$

Performing a Fourier transformation $\hat{b}_{\boldsymbol{k}\alpha} = \dfrac{1}{\sqrt{N}} \sum_i \hat{b}_{i\alpha}\, \mathrm{e}^{-\mathrm{i}\boldsymbol{k}\cdot\boldsymbol{R}_i}$ and diagonalizing the Hamiltonian matrix at each momentum point yields the magnon spectrum.

A2. Spin wave for 3-sublattice state

We now introduce spin-wave theory for generic 3-sublattice states. In this case, the spin state on the three sublattices (A,B,C) may differ and are generally not the standard $|1\rangle$ state. Therefore, a separate local basis rotation must be performed on each sublattice such that its respective ground state spin configuration aligns with the first basis vector of the local Hilbert space. In these rotated basis, the Gell–Mann matrices assume representations different from the standard one. We denote these new representations for sublattice S as λ^{mS} $(m = 1,\ldots,8; S = A,B,C)$. We then introduce three flavors of Schwinger bosons, $\hat{b}_{iA\alpha}, \hat{b}_{iB\alpha}, \hat{b}_{iC\alpha}$ corresponding to each sublattice. The model Hamiltonian of model can be decomposed into three parts based on the three types of nearest-neighbor bonds:

$$\hat{H} = \hat{H}_{AB} + \hat{H}_{BC} + \hat{H}_{CA}. \tag{A6}$$

Each part has an identical strcture. Using $\hat{H}_{AB}$ as an example, we have

$$\begin{aligned}\hat{H}_{AB} = &\sum_{\langle ij\rangle_{AB}} (T_{\alpha\beta}^{AB} \hat{b}_{iA\alpha}^\dagger \hat{b}_{jB\beta} + \mathrm{h.c.}) \\ &+ \sum_{\langle ij\rangle_{AB}} (\Delta_{\alpha\beta}^{AB} \hat{b}_{iA\alpha}^\dagger \hat{b}_{jB\beta}^\dagger + \mathrm{h.c.})\end{aligned}$$

$$+z_{AB}\sum_{i\in A}V^{AB}_{\alpha\beta}\hat{b}^{\dagger}_{iA\alpha}\hat{b}_{iA\beta}$$
$$+z_{AB}\sum_{i\in B}V^{BA}_{\alpha\beta}\hat{b}^{\dagger}_{iB\alpha}\hat{b}_{iB\beta}+E_0. \tag{A7}$$

Here, $z_{AB}=3$ is the coordination number for an AB-bond, and matrices $\boldsymbol{V}^{AB},\boldsymbol{\Delta}^{AB},\boldsymbol{T}^{AB}$ are defined as

$$\begin{cases} V^{AB}_{\alpha\beta}=\sum_{m=1}^{8}J^m(\lambda^{mA}_{\alpha\beta}-\lambda^{mA}_{00}\delta_{\alpha\beta})\lambda^{mB}_{00}, \\ T^{AB}_{\alpha\beta}=\sum_{m=1}^{8}J^m\lambda^{mA}_{\alpha0}\lambda^{mB}_{0\beta}, \\ \Delta^{AB}_{\alpha\beta}=\sum_{m=1}^{8}J^m\lambda^{mA}_{\alpha0}\lambda^{mB}_{\beta0}. \end{cases} \tag{A8}$$

After performing the Fourier transformation $\hat{b}_{\boldsymbol{k}S\alpha}=\sqrt{\frac{3}{N}}\sum_i\hat{b}_{iS\alpha}\,\mathrm{e}^{-\mathrm{i}\boldsymbol{k}\cdot\boldsymbol{R}_i}$ (where $S=A,B,C$), the Hamiltonian can be expressed as a 12×12 matrix $\mathcal{H}(\boldsymbol{k})$ in the basis of these bosonic operators. To diagonlize this matrix, one must solve the Bogoliubov–de Gennes eigenvalue problem $\Sigma\mathcal{H}(\boldsymbol{k})\boldsymbol{v}_i=E_i(\boldsymbol{k})\boldsymbol{v}_i$, where the metric Σ is given by

$$\Sigma=\begin{pmatrix}\boldsymbol{I}_6 & \\ & -\boldsymbol{I}_6\end{pmatrix}. \tag{A9}$$

The six eigenvalues $E_i(\boldsymbol{k})$ found at each momentum point correspond to the spin-wave excitation energies. Their associated eigenvectors $\boldsymbol{v}_i$ must satisfy the positive normalization condition $\boldsymbol{v}_i^{\dagger}\Sigma\boldsymbol{v}_i=1$. These six modes correspond to two magnon branches originating from each of the three sublattices.

Appendix B: Irreps of the group $G=U(1)\times Z_4^{PT}/Z_2$

The group $G=U(1)\times Z_4^{PT}/Z_2$ has one 1-dimensional irrep and infinite 2-dimensional irreps, as shown in Table B1. Each irrep is labeled by an integer $m\in\mathbb{Z}$, namely, the (abstract) value of the $U(1)$ 'charge'.

Table B1. Irreducible representation of the group $G=U(1)\times Z_4^{PT}/Z_2$ carried by magnon creation operators. Notice that $(PT)^2=(-1)^m$ is the spin parity (quantum number of $P_s=\mathrm{e}^{-\mathrm{i}\lambda^3\pi}$) with m the eigenvalue of $S_z=\lambda^3$.

	$\mathrm{e}^{-\mathrm{i}\lambda^3\theta}$	PT	Dimensionality
irrep-(0)	1	$1K$	1
irrep-(1)	$\begin{pmatrix}\mathrm{e}^{-\mathrm{i}\theta} & \\ & \mathrm{e}^{\mathrm{i}\theta}\end{pmatrix}$	$\begin{pmatrix}-1 & \\ 1 & \end{pmatrix}K$	2
⋮	⋮	⋮	⋮
irrep-(m)	$\begin{pmatrix}\mathrm{e}^{-\mathrm{i}m\theta} & \\ & \mathrm{e}^{\mathrm{i}m\theta}\end{pmatrix}$	$\begin{pmatrix}(-1)^m & \\ 1 & \end{pmatrix}K$	2
⋮	⋮	⋮	⋮

In the following, we illustrate that the spin-wave operators in the $SU(2)$ supersolid phase carry a 2-dimensional irrep labeled by $m=1$.

The $SU(2)$ supersolid phase is a three-sub-lattice order having the ground state $|\psi_A\rangle=|1\rangle,|\psi_B\rangle=|-1\rangle,|\psi_C\rangle=|0\rangle$. According to $SU(3)$ spin wave theory, each sublattice contributes two magnon bands. On sublattice-A ($|1\rangle$), the magnon creation operators are given by

$$\frac{1}{2}(\lambda^1-\mathrm{i}\lambda^2)=\begin{pmatrix}0&0&0\\1&0&0\\0&0&0\end{pmatrix},\quad \frac{1}{2}(\lambda^4-\mathrm{i}\lambda^5)=\begin{pmatrix}0&0&0\\0&0&0\\1&0&0\end{pmatrix}.$$

Similarly, on sublattice-B ($|-1\rangle$), the magnon creation operators are

$$\frac{1}{2}(\lambda^6+\mathrm{i}\lambda^7)=\begin{pmatrix}0&0&0\\0&0&1\\0&0&0\end{pmatrix},\quad \frac{1}{2}(\lambda^4+\mathrm{i}\lambda^5)=\begin{pmatrix}0&0&1\\0&0&0\\0&0&0\end{pmatrix};$$

and on sublattice-C ($|0\rangle$),

$$\frac{1}{2}(\lambda^1+\mathrm{i}\lambda^2)=\begin{pmatrix}0&1&0\\0&0&0\\0&0&0\end{pmatrix},\quad \frac{1}{2}(\lambda^6-\mathrm{i}\lambda^7)=\begin{pmatrix}0&0&0\\0&0&0\\0&1&0\end{pmatrix}.$$

These magnon operators carry nontrivial quantum numbers of the $U(1)=\{\mathrm{e}^{-\mathrm{i}\lambda^3\theta}\}$ group. For instance,

$$\begin{aligned}[\lambda^3,(\lambda^1\pm\mathrm{i}\lambda^2)]&=\lambda^3(\lambda^1\pm\mathrm{i}\lambda^2)-(\lambda^1\pm\mathrm{i}\lambda^2)\lambda^3\\&=\pm(\lambda^1\pm\mathrm{i}\lambda^2),\end{aligned} \tag{B1}$$

so $\frac{1}{2}(\lambda^1+\mathrm{i}\lambda^2)$ and $\frac{1}{2}(\lambda^1-\mathrm{i}\lambda^2)$ carry $U(1)$ 'charge' $+1$ and -1 respectively, namely,

$$\mathrm{e}^{-\mathrm{i}\lambda^3\theta}(\lambda^1\pm\mathrm{i}\lambda^2)\mathrm{e}^{\mathrm{i}\lambda^3\theta}=\mathrm{e}^{\mp\mathrm{i}\theta}(\lambda^1\pm\mathrm{i}\lambda^2).$$

Similarly, $(\lambda^6\pm\mathrm{i}\lambda^7)$ carry $U(1)$ 'charge' ±1. However, because $[\lambda_3,(\lambda^4\pm\mathrm{i}\lambda^5)]=\pm2(\lambda^4\pm\mathrm{i}\lambda^5)$, so $(\lambda^4\pm\mathrm{i}\lambda^5)$ carry 'charge' ±2, respectively.

On the other hand, under the action of PT, the magnon creation operators form pairs, namely,

$$\begin{aligned}(PT)(\lambda^1\pm\mathrm{i}\lambda^2)(PT)^{-1}&=+(\lambda^6\mp\mathrm{i}\lambda^7),\\(PT)(\lambda^6\pm\mathrm{i}\lambda^7)(PT)^{-1}&=-(\lambda^1\mp\mathrm{i}\lambda^2),\\(PT)(\lambda^4+\mathrm{i}\lambda^5)(PT)^{-1}&=-(\lambda^4-\mathrm{i}\lambda^5),\\(PT)(\lambda^4-\mathrm{i}\lambda^5)(PT)^{-1}&=-(\lambda^4+\mathrm{i}\lambda^5).\end{aligned}$$

Therefore, the pair of magnon operators $[(\lambda^1+\mathrm{i}\lambda^2),(\lambda^6-\mathrm{i}\lambda^7)]$ carries the 2-dimensional irrep ($m=1$) of the group $G=U(1)\times Z_4^{PT}/Z_2$. Similarly, the bases $[(\lambda^6+\mathrm{i}\lambda^7),-(\lambda^1-\mathrm{i}\lambda^2)]$ also carry the same irrep of G. But $[(\lambda^4+\mathrm{i}\lambda^5),-(\lambda^4-\mathrm{i}\lambda^5)]$ carried the irrep ($m=2$).

Appendix C: Alternative definition of the $U(2)$ symmetry group

In this work, we have modified the definition of λ^3,λ^8, to make sure that λ^3 fully represents the magnetic moment in the general convention. Under this convention, $|\pm1\rangle$, two bases of the sub-Hilbert space for single spin-1 site which can be connected with time-reversal operation, can take the role of $SU(2)$ generators, acting on the subspace span$\{|1\rangle,|-1\rangle\}$. This modification of Gell–Mann matrices may be more realistic to real magnetic systems, and become a key factor in the emergence of spin-2 excitations.

On the other hand, one can adopt the origin convention of $\lambda^{3,8}$, with $\lambda^3 = \frac{1}{2}S_z + \frac{3}{2}S_z^2 - I$, $\lambda^8 = (\frac{3}{2}S_z - \frac{3}{2}S_z^2 + I)/\sqrt{3}$, namely,

$$\lambda^3 = \begin{pmatrix} 1 & 0 & 0 \\ 0 & -1 & 0 \\ 0 & 0 & 0 \end{pmatrix}, \quad \lambda^8 = \frac{1}{\sqrt{3}} \begin{pmatrix} 1 & 0 & 0 \\ 0 & 1 & 0 \\ 0 & 0 & -2 \end{pmatrix},$$

and redefine the $SU(2)$ symmetry group to be generated by $\lambda^{1,2,3}$ which act on the subspace span$\{|1\rangle, |0\rangle\}$. Then the model Hamiltonian is modified as

$$H = J_3 \sum_{\langle ij \rangle} \sum_{\alpha=1}^{8} \lambda_i^\alpha \lambda_j^\alpha + J_2 \sum_{\langle ij \rangle} \sum_{m=1}^{3} \lambda_i^m \lambda_j^m + J_1 \sum_{\langle ij \rangle} \lambda_i^8 \lambda_j^8,$$

and the excitations including the Goldstone modes can carry S_z quantum numbers ± 1, and then can be detected in neutron scattering experiments.

Data availability statement

The data that support the findings of this study are openly available in Science Data Bank at https://doi.org/10.57760/sciencedb.j00113.00293.

Acknowledgements

We thank Qiang Luo, Han-Jin Shen, Rong Yu and Zhi-Yuan Xie for valuable discussions, and thank Yi Zhou and T. K. Ng for previous collaborations in related topics. This work was supported by the National Key Research and Development Program of China (Grant Nos. 2023YFA1406500 and 2022YFA1405300) and the National Natural Science Foundation of China (Grant Nos. 12374166 and 12134020). Computational resources have been provided by the Physical Laboratory of High Performance Computing at Renmin University of China.

References

[1] Leggett A J 1970 *Phys. Rev. Lett.* **25** 1543
[2] Kim E and Chan M 2004 *Nature* **427** 225
[3] Kim D Y and Chan M H W 2012 *Phys. Rev. Lett.* **109** 155301
[4] Boninsegni M and Prokof'ev N V 2012 *Rev. Mod. Phys.* **84** 759
[5] Murthy G, Arovas D and Auerbach A 1997 *Phys. Rev. B* **55** 3104
[6] Heidarian D and Damle K 2005 *Phys. Rev. Lett.* **95** 127206
[7] Melko R G, Paramekanti A, Burkov A A, Vishwanath A, Sheng D N and Balents L 2005 *Phys. Rev. Lett.* **95** 127207
[8] Wessel S and Troyer M 2005 *Phys. Rev. Lett.* **95** 127205
[9] Boninsegni M and Prokof'ev N 2005 *Phys. Rev. Lett.* **95** 237204
[10] Wang F, Pollmann F and Vishwanath A 2009 *Phys. Rev. Lett.* **102** 017203
[11] Jiang H C, Weng M Q, Weng Z Y, Sheng D N and Balents L 2009 *Phys. Rev. B* **79** 020409
[12] Wang F, Pollmann F and Vishwanath A 2009 *Phys. Rev. Lett.* **102** 017203
[13] Heidarian D and Paramekanti A 2010 *Phys. Rev. Lett.* **104** 015301
[14] Yamamoto D, Marmorini G and Danshita I 2014 *Phys. Rev. Lett.* **112** 127203
[15] Yamamoto D, Marmorini G and Danshita I 2015 *Phys. Rev. Lett.* **114** 027201
[16] Sellmann D, Zhang X F and Eggert S 2015 *Phys. Rev. B* **91** 081104
[17] Yamamoto D, Marmorini G, Tabata M, Sakakura K and Danshita I 2019 *Phys. Rev. B* **100** 140410
[18] Gao Y, Fan Y C, Li H, Yang F, Zeng X T, Sheng X L, Zhong R, Qi Y, Wan Y and Li W 2022 *npj Quantum Materials* **7** 89
[19] Xiang J, Zhang C, Gao Y, Schmidt W, Schmalzl K, Wang C W, Li B, Xi N, Liu X Y, Jin H, Li G, Shen J, Chen Z, Qi Y, Wan Y, Jin W, Li W, Sun P and Su G 2024 *Nature* **625** 270
[20] Haldane F 1983 *Phys. Lett. A* **93** 464
[21] Haldane F D M 1983 *Phys. Rev. Lett.* **50** 1153
[22] Buyers W J L, Morra R M, Armstrong R L, Hogan M J, Gerlach P and Hirakawa K 1986 *Phys. Rev. Lett.* **56** 371
[23] Gu Z C and Wen X G 2009 *Phys. Rev. B* **80** 155131
[24] Pollmann F, Turner A M, Berg E and Oshikawa M 2010 *Phys. Rev. B* **81** 064439
[25] Chen X, Gu Z C, Liu Z X and Wen X G 2013 *Phys. Rev. B* **87** 155114
[26] Chen X, Gu Z C and Wen X G 2011 *Phys. Rev. B* **83** 035107
[27] Liu Z X, Chen X and Wen X G 2011 *Phys. Rev. B* **84** 195145
[28] Liu Z X, Zhou Y, Tu H H, Wen X G and Ng T K 2012 *Phys. Rev. B* **85** 195144
[29] Liu Z X, Mei J W, Ye P and Wen X G 2014 *Phys. Rev. B* **90** 235146
[30] Greiter M and Thomale R 2009 *Phys. Rev. Lett.* **102** 207203
[31] Liu Z X, Tu H H, Wu Y H, He R Q, Liu X J, Zhou Y and Ng T K 2018 *Phys. Rev. B* **97** 195158
[32] Shi K, Zhang W and Liu Z X 2023 *Phys. Rev. A* **108** 033308
[33] Liu T, Wu Y H, Tu H H and Xiang T 2025 *Phys. Rev. B* **111** 205137
[34] Batista C D and Ortiz G 2001 *Phys. Rev. Lett.* **86** 1082
[35] Batista C D and and G O 2004 *Advances in Physics* **53** 1
[36] Sengupta P and Batista C D 2007 *Phys. Rev. Lett.* **98** 227201
[37] Tsunetsugu H and Arikawa M 2006 *J. Phys. Soc. Jpn.* **75** 083701
[38] Bhattacharjee S, Shenoy V B and Senthil T 2006 *Phys. Rev. B* **74** 092406
[39] Liu Z X, Zhou Y and Ng T K 2010 *Phys. Rev. B* **82** 144422
[40] Liu Z X, Zhou Y and Ng T K 2010 *Phys. Rev. B* **81** 224417
[41] Jin H K, Miao J J and Zhou Y 2019 *Phys. Rev. B* **100** 085101
[42] Sengupta P and Batista C D 2007 *Phys. Rev. Lett.* **99** 217205
[43] Sheng J, Hu J, Xu L, Wang L, Shi X, Chi R, Yu D, Podlesnyak A, Piyawongwatthana P, Murai N, Ohira-Kawamura S, Yuan H, Wang L, Mei J W, Liao H J, Xiang T, Wu L and Wang Z 2025 Preprint 2503.13888
[44] Marsaglia G 1972 *The Annals of Mathematical Statistics* **43** 645
[45] Remund K, Pohle R, Akagi Y, Romhányi J and Shannon N 2022 *Phys. Rev. Res.* **4** 033106
[46] Claudine L, Philippe M and Mila F 2011 *Introduction to Frustrated Magnetism* pp. 2197–4179 (Berlin, Heidelberg: Springer)
[47] Läuchli A, Mila F and Penc K 2006 *Phys. Rev. Lett.* **97** 087205
[48] Blankschtein D, Ma M, Berker A N, Grest G S and Soukoulis C M 1984 *Phys. Rev. B* **29** 5250
[49] Yao D, Zhang C, Xie Z Y, Fan Z and Deng Y 2025 *Phys. Rev. B* **111** 214403
[50] Muniz R A, Kato Y and Batista C D 2014 *Progress of Theoretical and Experimental Physics* **2014** 083I01
[51] Dong Z Y, Wang W and Li J X 2018 *Phys. Rev. B* **97** 205106
[52] Bauer B, Corboz P, Läuchli A M, Messio L, Penc K, Troyer M and Mila F 2012 *Phys. Rev. B* **85** 125116
[53] Arovas D P and Auerbach A 1988 *Phys. Rev. B* **38** 316